RSC Advances

PAPER

View Article Online
View Journal | View Issue

Cite this: *RSC Adv.*, 2023, **13**, 251

Targeting biomarkers in the gas phase through a chemoresistive electronic nose based on graphene functionalized with metal phthalocyanines†

Sonia Freddi, [ab] Camilla Marzuoli,‡§[a] Stefania Pagliara, [a] Giovanni Drera[a] and Luigi Sangaletti *[a]

Electronic noses (e-noses) have received considerable interest in the past decade as they can match the emerging needs of modern society such as environmental monitoring, health screening, and food quality tracking. For practical applications of e-noses, it is necessary to collect large amounts of data from an array of sensing devices that can detect interactions with molecules reliably and analyze them *via* pattern recognition. The use of graphene (Gr)-based arrays of chemiresistors in e-noses is still virtually missing, though recent reports on Gr-based chemiresistors have disclosed high sensing performances upon functionalization of the pristine layer, opening up the possibility of being implemented into e-noses. In this work, with the aim of creating a robust and chemically stable interface that combines the chemical properties of metal phthalocyanines (M-Pc, M = Fe, Co, Ni, Zn) with the superior transport properties of Gr, an array of Gr-based chemiresistor sensors functionalized with drop-cast M-Pc thin layers has been developed. The sensing capability of the array was tested towards biomarkers for breathomics application, with a focus on ammonia (NH_3). Exposure to NH_3 has been carried out drawing the calibration curve and estimating the detection limit for all the sensors. The discrimination capability of the array has then been tested, carrying out exposure to several gases (hydrogen sulfide, acetone, ethanol, 2-propanol, water vapour and benzene) and analysing the data through principal component analysis (PCA). The PCA pattern recognition results show that the developed e-nose is able to discriminate all the tested gases through the synergic contribution of all sensors.

Received 29th November 2022
Accepted 12th December 2022

DOI: 10.1039/d2ra07607a

rsc.li/rsc-advances

Introduction

Gas sensor development has been attracting the interest of the research community for many years, boosted by market demands. Only recently have electronic noses (e-noses) appeared on the market, due to their potentially wide range of applications[1] and to the need for overcoming the limits of single sensor development, improving the device selectivity towards specific target gas molecules. Furthermore, with respect to a single sensor, an e-nose is a more suitable choice whenever the data analysis requires a technology able to classify a sample according to pre-determined criteria, rather than providing information about some specific components.[2] Finally, the use of machine learning algorithms is providing reliable solutions and alternative routes for the analysis and the classification of data obtained from e-noses.[3] In this perspective, e-noses are mainly exploited for food and beverage quality tracking (*e.g.* classification of fresh *vs.* adulterated food, product origin and quality tracking),[4–9] environmental monitoring,[4,9] and breathomics (*e.g.*, classification of sick patients *vs.* healthy subjects for specific pathologies).[9–12]

In particular, breathomics, or breath analysis, holds great promise to deliver rapid, non-invasive and low-cost diagnosis of diseases, playing a major role in screening campaigns for those pathologies where an early diagnosis is crucial for the success of the treatment, such as lung cancer. Breath analysis is based on the fact that the quantity and the quality of the volatile organic compounds (VOCs) present in the exhaled breath of healthy patients are different from those found in the exhaled breath of sick patients and that each pathology is related to the presence of specific gas molecules (*i.e.* the biomarkers) in a fixed quantity.[13,14]

[a]*Department of Mathematics and Physics, Surface Science and Spectroscopy Lab@ I-Lamp, Università Cattolica del Sacro Cuore, Via della Garzetta 48, 25123 Brescia, Italy*

[b]*Department of Chemistry, Division of Molecular Imaging and Photonics, KU Leuven, Celestijnenlaan 200F, 3001 Leuven, Belgium*

† Electronic supplementary information (ESI) available. See DOI: https://doi.org/10.1039/d2ra07607a

‡ Current address: Center for Nano Science and Technology@PoliMi, Istituto Italiano di Tecnologia, Via Giovanni Pascoli 70/3, 20133 Milano, Italy.

§ Department of Physics, Politecnico di Milano, P.zza L. Da Vinci 32, 20133 Milano, Italy.

Currently, commercially available e-noses are mainly based on conducting polymers or metal oxide sensing devices that still present several drawbacks, including a high operation temperature and therefore a high-power consumption, and poor stability.[1,15] Therefore, researcher started to look into new materials to develop e-noses, including sensing layers based on nanostructured carbon, such as carbon nanotubes (CNT), graphene (Gr), graphene oxide (GO), and reduced graphene oxide (rGO). CNTs have already been tested in e-noses, disclosing their potentialities for breathomics,[11,16–19] and for food/beverage quality tracking.[20,21] On the other hand, studies of e-noses based on a set of graphene layers are virtually missing.

Early claims of the sensing capabilities of Gr layers have been reported,[22] but over the years they have been replaced by the use of GO, rGO, and related nanocomposites.[23–25] Starting from GO, partial removal of oxygen groups, leading to rGO, can be achieved by chemical, thermal, or ultraviolet-assisted process, resulting in gas sensing performance comparable or superior to that of pristine graphene, as the oxygen-related defects behave as chemically active sites. However, GO-based sensing layers present some drawbacks in terms of sample reproducibility due to the poor control on surface functionalization.[23,24]

In turn, Gr layers allow for a precise determination, and therefore control of the electronic properties. For instance, Gr band structure mapping enabled by angle-resolved photoemission spectroscopy (ARPES) provides unambiguous evidence of the extent and character (*i.e.* p-type or n-type) of doping, determined either by the interaction with the substrate or by the functionalization, and of the integrity of the electronic structure when exposed to molecules present in the ambient air, such as oxygen and nitrogen.[26,27]

In this perspective Gr represents a more reliable layer to develop sensing platforms, provided that proper and effective functionalization strategies are introduced to enhance Gr sensing properties. In particular, recent studies have demonstrated the possibility to develop highly sensitive Gr layers upon functionalization,[28–32] disclosing important progress in the field of specific molecule sensing in the gas phase that, in turn, can be considered as a promising starting point for the development of graphene-based e-noses. So far only few Gr-based e-noses driven in a FET configuration have been reported,[33–35] which requires micro-electronic grade preparation of the device, or e-noses based on capacitors.[36] In turn, Gr-based e-noses in a chemiresistive configuration can be assembled following facile preparation routes, but they are still missing.

In the present work, a set of graphene layers on silicon nitride insulating substrates has been functionalized with metal phthalocyanines (M-Pc), with the aim to create a robust and chemically stable interface that combines the chemical (*i.e.* chemosensing) properties of M-Pc with the superior transport properties of Gr for the development of Gr-based chemiresistors.

M-Pc layers are already used for gas sensing and Cu- and Co-Pc, followed by Zn-, Ni- and Fe-Pc, are the most exploited M-Pc for gas sensing application.[37–49] On the other hand, tentative functionalization of graphene-based layers with phthalocyanines has been recently reported, but mostly graphene oxide and the π–π interaction between phthalocyanine and graphene oxide have been considered,[50–52] rather than graphene.

Generally speaking, the functionalization of pristine graphene layers with phthalocyanines has not been investigated to a large extent, and sensors based on graphene layers functionalized with phthalocyanines have not yet been introduced as the sensing array into an e-nose.

In detail, we prepared an array of 5 chemiresistive sensors: one sensor based on pristine graphene (Gr_pristine) and 4 graphene sensors functionalized with M-Pc (M = Co, Ni, Zn and Fe), with the aim to test this array of graphene sensing layers as an e-nose. In particular, these M-Pc have been selected due to their reported good sensing performances.[49,53–56]

The M-Pc layers have been deposited on graphene from a solution by dropcasting, a facile, low cost, and easy functionalization technique. In view of possible applications in the field of breathomics testing of the sensor array has been carried out with ammonia as target gas molecule. Ammonia in the exhaled breath is recognized as the biomarker of both liver and kidney failure and chronic obstructive pulmonary diseases.[57,58] Indeed, ammonia concentration around 10 ppb can be found in the exhaled breath of healthy subjects, while in case of liver or kidney malfunctioning this concentration can rise up till 1 ppm.[14] Furthermore, ammonia, along with NO_2, is usually regarded as a testing gas for novel nanocarbon based sensors.[22,59] Following this choice, calibration curves have been drawn, discussing the sensing mechanism of the sensors, in particular of the Gr_CoPc layer, which displayed a distinctive behavior with respect to the other sensors in the set. Then the discrimination capability of the array has been tested, carrying out exposures to several possible interfering gases (acetone, ethanol, water vapour, 2-propanol, benzene, sodium hypochlorite and hydrogen sulfide) and analysing the data through principal component analysis (PCA) in order to assess the role of each sensor in the discrimination process.

Incidentally, also the interfering gas molecules listed above are known to be biomarkers for several pathologies such as diabetes (acetone),[60,61] lung cancer (2-propanol, benzene and ethanol),[62] asthma (hydrogen sulfide),[63,64] and cystic fibrosis (sodium hypochlorite).[65]

Finally, in the present approach the parallel screening of the Gr-based sensors response upon exposure to these target gas molecules can disclose new sensing layers for targeting specific molecules in case of remarkable response of one sensor over the others.

Experimental

Sample preparation

5 different samples of graphene on 10 × 10 mm^2 Si/Si_3N_4 substrates make up the electronic nose. One of the samples is pristine graphene (Gr_pristine) and 4 of them are functionalized *via* dropcasting of cobalt (CoPc), iron (FePc), nickel (NiPc), and zinc (ZnPc) metal phthalocyanine solutions. Graphene on Si/Si_3N_4 substrates have been purchased from Graphenea, while phthalocyanine powders from Sigma-Aldrich.

Batch-to-batch or sample-to-sample variation is primarily affected by the quality of the graphene layers. Therefore, Gr layers with comparable resistivity have been selected for the array after proper functionalization (see Table SI of the ESI†).

The phthalocyanine powders have been dissolved into acetone (NiPc) or ethanol (all the other molecules) with a concentration of 0.1 mM and then, after 10 minutes of sonication, 15 droplets of the solution have been dropcasted on the graphene layer (Fig. 1a) and have been left to dry upon solvent evaporation in air.

The choice of the solvent and concentration was made on the basis of ref. 66. A cross-sectional sketch of the functionalized layers is shown in Fig. 1b.

For a preliminary investigation of batch-to-batch reproducibility, additional samples have been prepared on selected layers, functionalized with NiPc and CoPc (hereafter labelled as Gr_NiPc_A, B and C, Gr_CoPc_A, B and C).

Sample characterization

Raman spectroscopy and atomic force microscopy (AFM) have been performed to characterize the samples.

Raman spectra and micro-Raman maps have been collected on a Renishaw-Invia system, equipped with a 633 nm laser source.

The laser light has been focused onto the sample with a 100× objective. An 1800 lines per mm grating and a laser power of 5 mW have been used for the measurements.

AFM images have been acquired with a Park NX 10 AFM system in non-contact mode in air–solid interface with a tip operating at a resonance frequency of about 300 kHz. All the images processing has been performed using the Gwyddion software.[67]

Baseline resistance and AFM measurements have been carried out also on the three additional samples of Gr_NiPc and Gr_CoPc (Gr_NiPc_A, B and C, Gr_CoPc_A, B and C).

Gas sensing measurement

To measure the chemoresistive response of the samples to the selected gases, electrical contacts have been made with silver paint stripes at the opposite sides of the sample. The samples have then been mounted on a properly designed platform (the e-nose) able to host up to 8 sensors, for the simultaneous

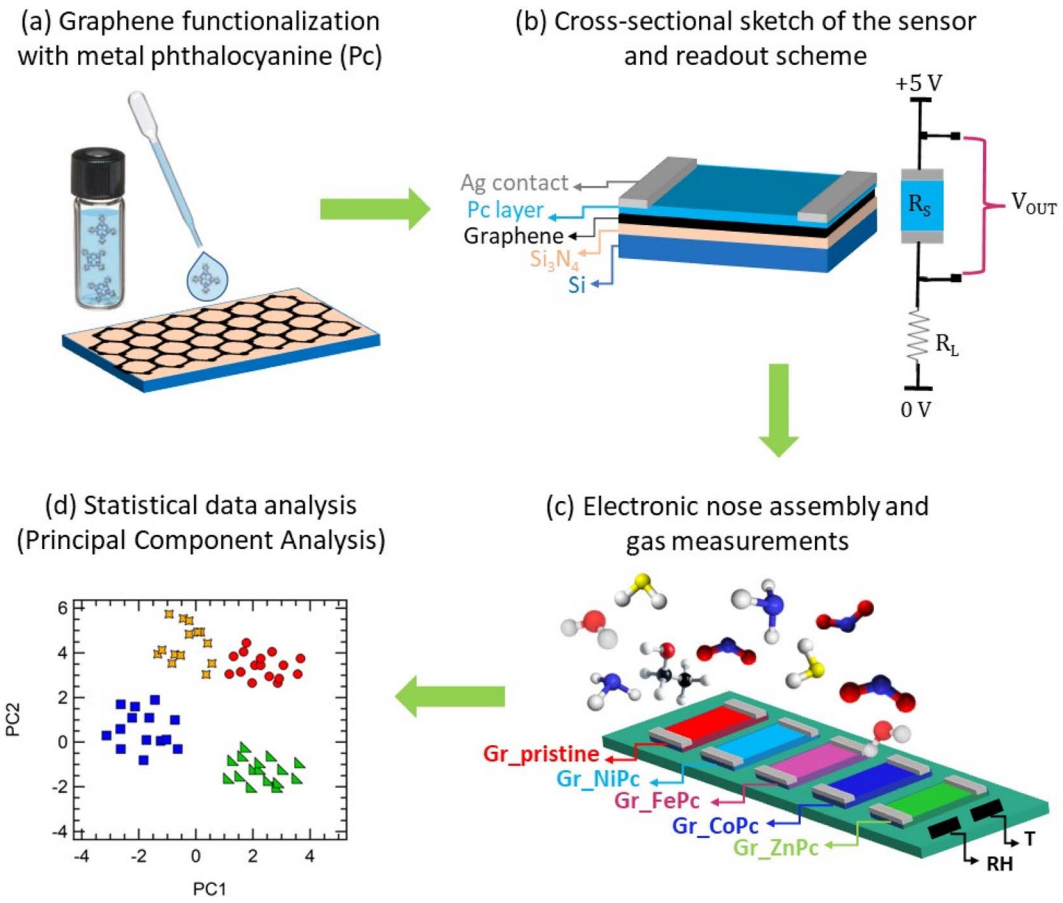

Fig. 1 Summary of the methodology. (a) Graphene layers are functionalized with metal phthalocyanine *via* dropcasting. (b) Cross sectional sketch of the layers after silver contact have been made and chemiresistor readout scheme of each layer. (c) Schematic representation of the electronic nose, assembled with a pristine graphene layer (red) and four phthalocyanines functionalized samples: NiPc (light blue), FePc (purple), CoPc (blue) and ZnPc (green). Relative humidity (RH) and temperature (*T*) sensors are mounted on the array, as well. (d) Data collected from the e-nose are analysed with PCA in order to obtain discrimination of the target gases molecules.

detection of all sensors response during gas exposures. With this set-up, the present platform allows for a direct comparison of the behaviour of the sensors under the same environmental conditions. Two commercial sensors have also been added to the platform: a relative humidity (RH) sensor (humidity sensor HIH-4000 series – Honeywell Sensing) and a temperature sensor (Thermistor NTC PCB 5K – Murata). A schematic representation of the e-nose is shown in Fig. 1c.

The sensor signals have been acquired using dedicated software, written in the LabVIEW environment. The gas sensing characteristics have been analysed by exploiting the chemo-resistive responses upon gas exposure. The basic electronic circuit for chemiresistor gas sensing measurements consisted of a load resistor (R_L) in series with the sensor, to which a constant voltage ($V = 5$ V) is applied. By monitoring the output voltage (V_{OUT}) across the sample, the sensor resistance R_S is measured. A scheme of the readout circuit developed for each sensor is shown in Fig. 1b. Therefore, the chemo-resistive responses have been evaluated as: $\Delta R/R_0 = (R - R_0)/R_0$, where R_0 is the baseline sensor resistance before exposure, while $\Delta R = R - R_0$ is the resistance variation occurring during gas exposure.

Gas exposures have been carried out at room temperature in a sealed custom made chamber, by introducing a mixture of synthetic air with a selected concentration of the analyte under investigation. Two cylinders have been used to feed the chamber through programmable mass-flow controllers (MKS Instruments) operating in a 200–500 sccm range. For ammonia exposures, the first cylinder (certified by SIAD Spa) has been loaded with 47 ppm of ammonia in synthetic air, while the second has been loaded with synthetic air alone (SIAD Spa) and used to change the overall concentration of ammonia in the chamber. Gas from both cylinders was pre-mixed before entering the chamber. During measurements the overall RH was (50 ± 10)%. Exposure time has been set around 1 minute and after each exposure the chamber has been purged by flushing it with synthetic air until the initial resistance value of the sensors has been restored. A scheme of the set-up is reported in Fig. S1.† This procedure has also been exploited for the other tested analytes, *i.e.* hydrogen sulfide, benzene, acetone, 2-propanol and ethanol.

Regarding ammonia, on the basis of several exposures calibration curves for each sensor have been obtained by plotting the sensor response $\Delta R/R_0$ *versus* the gas concentration.

Statistical data analysis

Data collected with the electronic nose have been analysed with a multivariate statistical approach, *i.e.* principal component analysis (PCA), implemented into the R software. PCA is an unsupervised statistical method that allows for the reduction of the problem dimensionality maximizing the variance; indeed, it redistributes the total response in a set of principal orthogonal components (PCs); PC1 represents the dimension with the greatest variance, PC2 the second greatest variance, and so on. The aim of this analysis is to achieve in a 2D or 3D space a clear discrimination of the gases (Fig. 1d). In this work, data to feed the PCA has been pre-treated only with the column mean-centring. For the PCA analysis, an overall set of 52 exposures to 8 different gases has been considered.

Results and discussion

The samples have been characterized through Raman and AFM measurements.

The Raman spectrum of pristine graphene (Fig. 2 (red curve)) shows the characteristic peaks of graphene: the G and 2D band. The G band, located at 1590 cm^{-1}, is ascribed to the C–C stretching of sp^2 hybridized carbon atoms in the graphene lattice.[68] The 2D peak around 2648 cm^{-1} is a second order Raman scattering process and it is related to the breathing mode of carbon atoms in the plane of graphene.[68]

Regarding the band around 1330 cm^{-1}, it probably comes from two different contributions: as can be seen in the black curve of Fig. 2, silicon nitride substrate has a band in the same position (see also ref. 69), but also the D-band related to defects in graphene could be found around 1330 cm^{-1}.[68] Since the monolayer graphene is not highly defective, we could expect that the silicon nitride broad band dominates the feature around 1330 cm^{-1} in the Gr_pristine spectrum. Regarding the functionalized graphene samples, the G-band is well detectable

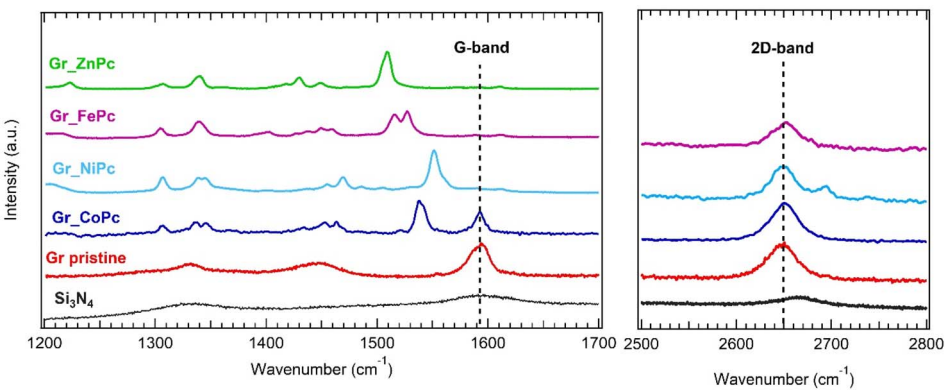

Fig. 2 Representative Raman spectra of Si_3N_4 substrate (black), graphene on Si/Si_3N_4 pristine (red) and with cobalt (blue), nickel (light blue), iron (purple), zinc (green) phthalocyanine. The 2D band of the samples with the Zn compounds could not be detected due to a strong luminescence in that spectral region.

in the Gr_CoPc sample, while in the other samples it is still detectable though with a very low intensity compared to all the other peaks in the spectra. This is an indication of a lower thickness of the molecule layer for the Gr_CoPc sample with respect to the other functionalized samples. Furthermore, considering the high intensity of the Pc related peaks, we assume that the ZnPc, FePc and NiPc are arranged in a multi-layer structure.

The presence of graphene is in any case confirmed by the 2D band, which is always detectable for all samples except for Gr_ZnPc, where a strong luminescence induced by the 633 nm laser beam irradiation is expected for the Zn-based complexes,[70] overwhelming the intensity of the Gr 2D band. All the peaks not related to graphene and present in the functionalized samples could be ascribed to the phthalocyanine molecules (see also Fig. S2†).

Fig. S3† shows representative images of the samples in a 3 × 3 μm^2 region. Pristine graphene (Fig. S3a†) shows the typical edges of a transferred graphene layer.

Topographic images representative of the Gr_CoPc, Gr_FePc and Gr_NiPc surfaces, shown in Fig. S3b, c and d,† respectively, display a quite uniform distribution of the phthalocyanine molecules on the layer, while regarding Gr_ZnPc the layer presents some agglomerates on the surface, ascribable to not well dissolved phthalocyanines.

Reproducibility of the batch-to-batch preparation in terms of the baseline resistance, before and after functionalization, and of the roughness of the prepared layers, obtained from several AFM images, have been confirmed, investigating the three additional samples of Gr_CoPc and Gr_NiPc (Gr_CoPc_A, B and C, Gr_NiPc_A, B and C) and comparing the result with those obtained from the chemiresistors equipping the e-nose (Gr_CoPc and Gr_NiPc). Results are reported in Tables SII and SIII,† respectively.

Gr_CoPc, Gr_NiPc, Gr_ZnPc, Gr_FePc and a pristine Gr chemiresistors on the e-nose (schematic representation reported in Fig. 3a) have been simultaneously exposed to ammonia.

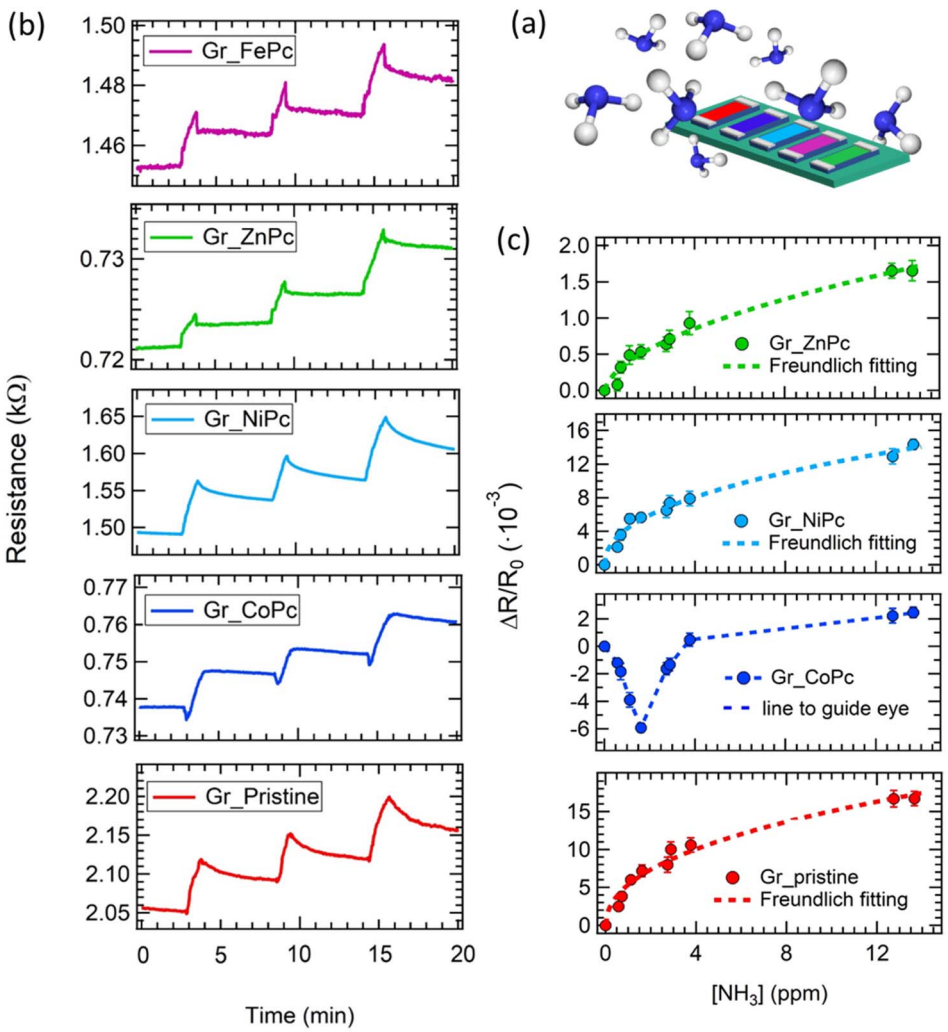

Fig. 3 (a) Schematic view of the sensor array exposed to ammonia. (b) Response of the sensor array to 64 ppm, 49 ppm and 72 ppm ammonia exposures. (c) Calibration curves interpolated with a Freundlich fit; for the Gr_CoPc sample, no fit is reported, but a line to guide the eyes has been added. Error bars represent standard deviation of the mean response obtained from three exposures to the same ammonia concentration.

As an example of the dynamical response of the array, the resistance change measured upon three exposures to high ammonia concentrations (*i.e.* 64 ppm, 49 ppm and 72 ppm) is shown in Fig. 3b. The exposure time has been set around 1 minute.

First of all, a quick response is observed for all samples (*i.e.* in a few seconds range) and most of the sensors increase their resistance upon ammonia exposure, disclosing an overall p-type behaviour; the exception is represented by the Gr_CoPc sensor, which exhibits at first, a decrease of the resistance is observed, but after few seconds the resistance starts to increase.

The high concentration used to perform such exposures does not permit a complete recovery in short time, but for concentrations below 15 ppm the recovery is achieved in about 3–5 minutes (see Fig. S4 and Table SIV†).

In order to draw the calibration curve in a concentration range of interest for e-nose applications, a sequence of exposures to ammonia at low concentrations (from 0.5 ppm to 13.5 ppm) has been carried out. The calibration curves of all sensors are shown in Fig. 3c, with the exception of the Gr_FePc chemiresistor, which did not display any response to NH_3 for concentrations below 8 ppm (see also Fig. S4†). A Freundlich isotherm ($\Delta R/R_0 = A[NH_3]^{pow}$) is used to interpolate the data (except for those obtained from the Gr_CoPc layer), and the fitting parameters are reported in Table SV.† The detection limit (dl), reported in Table SVI has been evaluated according to the formula: $3[NH_3]/((R - R_0)/\sigma)$,[71] where σ is the fluctuation of the electrical signal. In particular a detection limit of 0.17 ppm, 0.05 ppm, 0.05 ppm, 8 ppm and 0.03 ppm has been found for Gr_pristine, Gr_NiPc, Gr_ZnPc, Gr_FePc, and Gr_CoPc, respectively.

The calibration curves present a sublinear behaviour, which is quite common for gas sensors with carbon-based materials.[16,72] From the comparison of calibration curves it is clear that functionalization does not always enhance the response to ammonia; for instance, the response at the highest concentration (*i.e.* 13.5 ppm) of Gr_NiPc is higher than for the pristine sample, but the response of all the other sensors is lower, and no response at all is observed for the Gr_FePc. On the other hand, the detection limit is always better for the functionalized samples, except for the Gr_FePc sensor.

Rather than being detrimental to gas sensing, this variability among sensing response to different target gas molecules is a quite an important issue for data analysis and classification with machine learning algorithms.

A comparison with literature works has been performed in terms of sensitivity (*i.e.* sensor response percentage normalized over the concentration: $(\Delta R/R_0 \times 100)/[NH_3]$) and detection limit: the results obtained for the five developed sensors are in line with both graphene-based sensors,[28,29,73–80] and reduced graphene oxide functionalized with metal phthalocyanine molecules,[81–84] as can be found in Table SVII.†

As for the sensing mechanisms, the resistance increase upon ammonia exposure indicates that the Gr, Gr_FePc, Gr_NiPc, and Gr_ZnPc layers are p-type, consistently with the fact that the electron injection from ammonia reduces the density of holes in these layers.

The behaviour observed for Gr_CoPc is different and can be rationalized also at the light of the sensing of a CoPc chemiresistor layer exposed to ammonia. In this regard, a sample made of CoPc only has been prepared by drop-casting 15 drops of a CoPc solution on a glass substrate. Unlike graphene, glass is assumed to be an inert substrate without any electronic coupling with the Pc film, thus the observed response to gas exposure is related to the behaviour of the Pc film alone. Exposures to different ammonia concentrations have been carried out and the results are shown in Fig. S5.† The CoPc molecule layer decreases its resistance upon ammonia exposure, thus displaying an n-type semiconductor behaviour.

In literature, only the case of p-type graphene functionalized with p-type Pc is discussed by Guo *et al.*,[84] while results on n-type Pc have not yet been reported. Furthermore, the case reported in ref. 84 is different from our case; indeed, there CoPc and rGO were mixed together, while in our case the CoPc molecules form a layer onto the graphene substrate.

A possible sensing mechanism for Gr_CoPc exposed to ammonia is schematized in Fig. 4. Due to the presence of oxygen, pristine graphene in air is considered as a p-type material, thus the Fermi level is below the Dirac point, while n-type doping for CoPc has been experimentally observed,

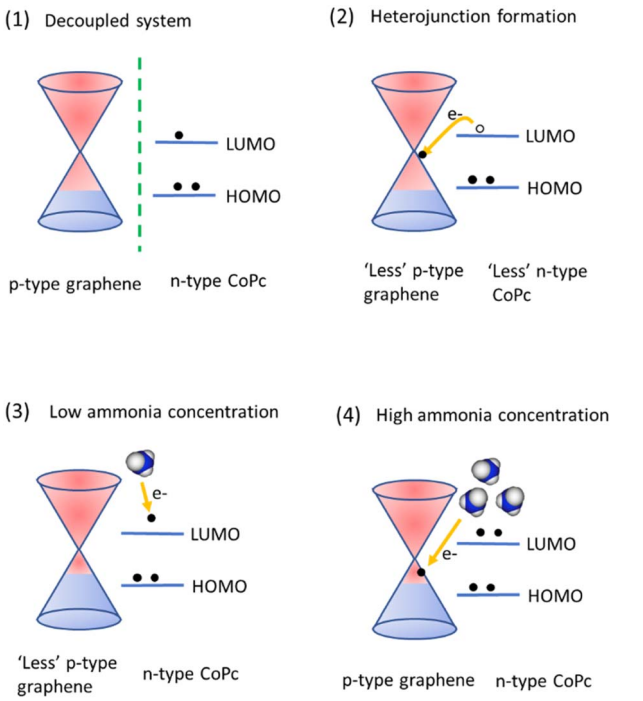

Fig. 4 Schematic representation of the sample formation and sensing mechanism in the case of ammonia exposure for a Gr_CoPc sensor. (1) In air, considering the uncoupled situation, graphene is a p-doped material, while the CoPc are n-type. (2) After the dropcasting, a junction is formed between graphene and CoPc. (3) In low ammonia concentration regime, NH_3 molecules interact with CoPc with a higher probability. (4) In high ammonia concentration regime, NH_3 starts to interact with the graphene layer. Ammonia molecules are represented with blue (N) and white (H) spheres. Filled states of Gr are shown in blue, whereas empty states are shown in red.

where the HOMO is filled, and electrons are also found in the LUMO (case (1) in Fig. 4).

DFT calculations carried out on a Gr_CuPc system reports that the HOMO is at lower energy with respect to the Fermi level of Gr, while the LUMO is above the graphene Fermi level;[85] assuming that this holds also for our CoPc case, the CoPc LUMO can be set above Fermi level of graphene.

Upon dropcasting the CoPc on the graphene layer, a heterojunction is formed, and the electrons in the CoPc LUMO drift towards graphene in order to align the respective states (case (2) in Fig. 4).

Once the equilibrium is reached, the graphene is now "less" p-type doped than in case 1 (decoupled system) and consequently the CoPc molecule layer is less n-type doped. Let us now analyse the case when ammonia is adsorbed at the sample surface considering both low and high ammonia concentrations.

Considering that the Gr layer is not completely covered by CoPc, as can be deduced by Raman map measurements collected on the sample and shown in the ESI (Fig. S6†), in a low concentration regime, ammonia results to interact preferably with the n-type phthalocyanine, donating electrons to them, thus leading to the experimentally observed resistance decrease. When ammonia concentration increases, more molecules reach the sample surface, saturating the phthalocyanines adsorption sites and therefore interacting mostly with graphene. Ultimately, this leads to the experimentally observed p-type behaviour, with an increase of the resistance value.

To support this claim, $\Delta R/R_0$ upon different ammonia concentration exposures has been evaluated as a two steps process (see ESI† file for further information): $(\Delta R/R_0)_{neg}$ and $(\Delta R/R_0)_{pos}$ as shown in Fig. 5a, and the results are shown in Fig. 5b and c. $(\Delta R/R_0)_{neg}$ is related to a n-type behaviour, *i.e.* CoPc layer, while $(\Delta R/R_0)_{pos}$ is the trend expected for a p-type layer, *i.e.* graphene.

Fig. 5b clearly shows that the $(\Delta R/R_0)_{neg}$ value decreases till a threshold concentration value (around 10 ppm), and then remains constant.

This behaviour is compatible with a saturation of the available sites in the n-type doped region of the sample, *i.e.* the CoPc layer. In contrast, the $(\Delta R/R_0)_{pos}$ value is zero in the 0–1 ppm range and beyond this range increases with concentration, suggesting that at first the p-type contribution is negligible, then in the 1–10 ppm range this behaviour is comparable with the n-type one, since the absolute value of the response is the same; finally, starting from 10 ppm concentration, the p-type response is dominant.

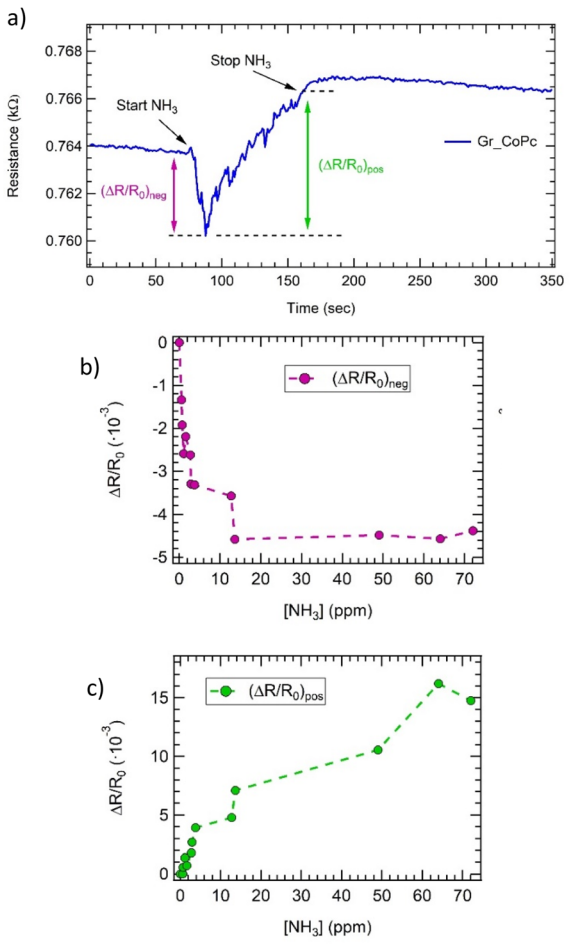

Fig. 5 (a) Schematic representation of how $(\Delta R/R_0)_{neg}$ and $(\Delta R/R_0)_{pos}$ are evaluated for an ammonia exposure of Gr_CoPc. (b) $(\Delta R/R_0)_{neg}$ as function of the ammonia concentration; (c) $(\Delta R/R_0)_{pos}$ as function of the ammonia concentration. Dashed lines are reported to guide the eyes through the trend.

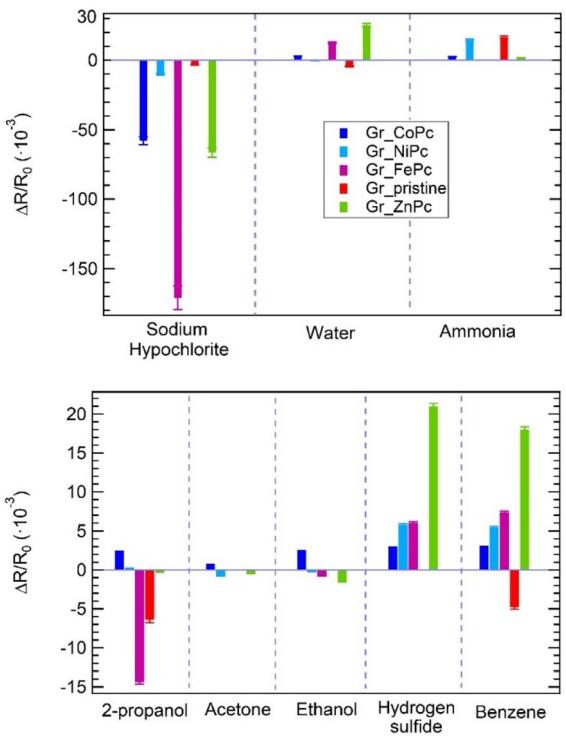

Fig. 6 Response of the sensor array to selected target molecules. Sodium hypochlorite (0.5 ppm), water (1000 ppm) and ammonia (13.5 ppm) (top panel); 2-propanol (40 ppm), acetone (40 ppm), ethanol (37 ppm), benzene (1 ppm), and hydrogen sulfide (2.5 ppm) (bottom panel).

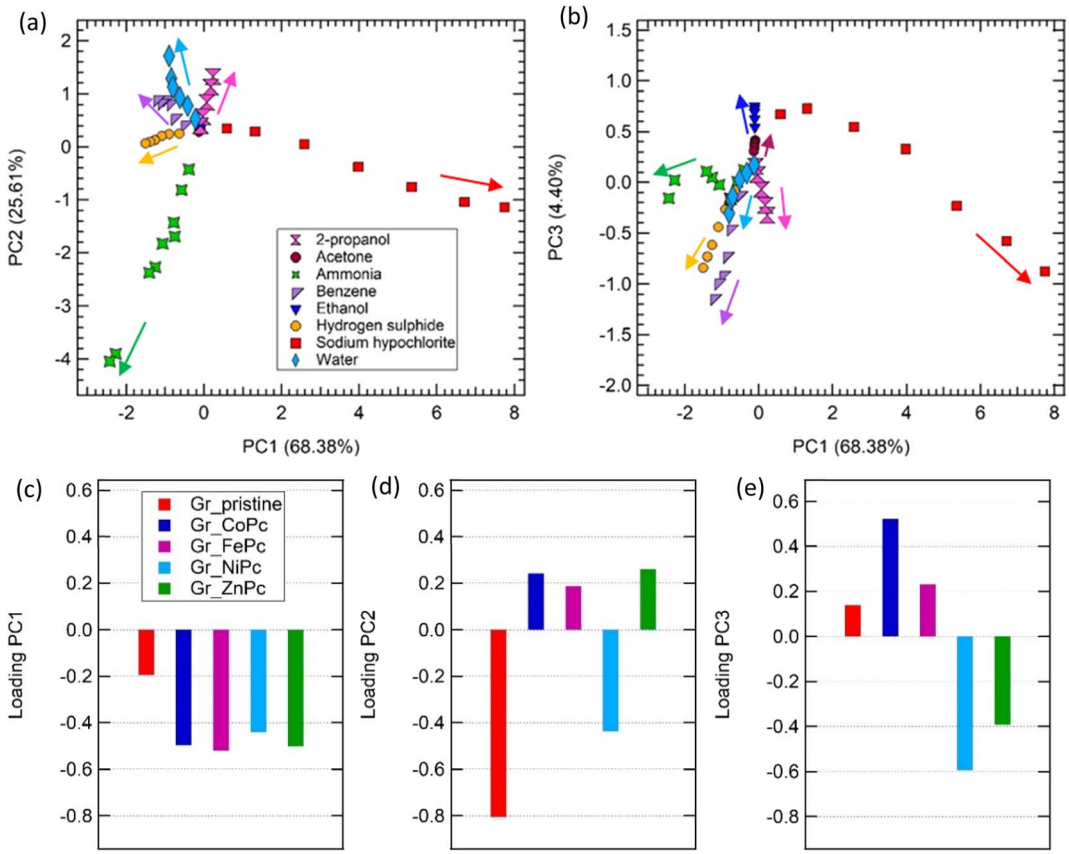

Fig. 7 PCA of the sensor array responses to exposure to hydrogen sulfide (0–2.5 ppm), benzene (0–1 ppm), ammonia (0–13.5 ppm), water (0–1000 ppm), acetone (0–40 ppm), ethanol (0–37 ppm) and 2-propanol (0–40 ppm) concentrations. PC2 *vs.* PC1 (a) and PC3 *vs.* PC1 (b). The arrows indicate the increasing concentration trend. Loadings on PC1 (c); loadings on PC2 (d); loadings on PC3 (e).

The sensing mechanism suggested for the Gr_CoPc layer is likely to occur also for the other samples, although the switch from negative to positive $\Delta R/R_0$ is not observed, as NiPc, FePc, and ZnPc are recognized as p-type compounds,[86–88] thereby displaying a behavior similar to that presented by p-type pristine graphene layers in air (Fig. 3c).

Datasets similar to those shown for ammonia in Fig. 3b have been collected for exposures to acetone, ethanol, benzene, 2-propanol, sodium hypochlorite, hydrogen sulfide and water.

Results are summarized in the histograms of Fig. 6, which shows the responses of the sensors array to the 8 selected target molecules expressed as the sensor response $\Delta R/R_0$ evaluated for the highest concentration tested.

All the sensors changed their resistance during exposure to all gases which have been tested, except for pristine graphene exposed to hydrogen sulfide, ethanol and acetone; indeed, in these cases a resistance change has not been observed.

In general, the whole sensor array shows a relevant response, especially to sodium hypochlorite, water and ammonia.

It is interesting to notice that, although Gr_pristine shows one of the best responses to ammonia, its response to the other gases is not the highest, indicating that the functionalization leads to an increase in the selectivity of the sensor array, required also by the statistical methods for the data analysis.

Furthermore, the possibility to test all the sensors in the same conditions, helps to identify the sensors with the best performances: in this array Gr_FePc is promising for 2-propanol and sodium hypochlorite detection, while Gr_ZnPc shows a huge response to hydrogen sulphide and benzene, as compared to the other sensors.

In order to enrich the data set, exposures to different concentrations of the same gas have been considered (see Table SVIII† for the concentration range) and PCA has been carried out on the sensors' responses; the results are shown in Fig. 7. Considering the space generated by PC1 and PC2 (Fig. 7a), not only the set of points ammonia is well separated from the other gases, but also all gases are clearly discriminated in the space, with an overlap of the acetone, 2-propanol and ethanol contributions only.

Taking into account also the third component (Fig. 7b, PC3 *vs.* PC1), this overlapping can be avoided and also these three compounds are clearly separated in the PCA space. Furthermore, as it has been previously observed on arrays based on CNTs,[11,89] a concentration trend is established: going towards the centre of the reference system, the gas concentration decreases. It is worth to mention that although the developed sensors do not show a particular high response to ammonia, when their response is combined in the PCA analysis, the whole

array is able to completely discriminate ammonia from the other gas contribution.

Of note, the present electronic nose is able to discriminate also the VOCs that usually are difficult to detect and discriminate with carbon-based sensors, such as acetone, ethanol and 2-propanol. Indeed, for instance considering carbon-nanotubes, it has been proved that these compounds do not provide an effective charge transfer to the bare carbon-based surfaces and a proper functionalization is required.[90]

Finally, loading plots for PC1, PC2, and PC3 help clarify the role of each individual sensor into the discrimination of target gas molecules. As shown in Fig. 7c, all the sensors equally contribute to PC1 loadings, except for Gr_pristine, which contributes to a minor extent. Therefore, 4 out of 5 sensors are clearly involved in the discrimination of sodium hypochlorite from all the other gas contributions along the PC1 axis of the PC1–PC2 space. PC2 loadings are dominated by the pristine contribution, but Gr_NiPc plays an important role too in the discrimination along PC2 (Fig. 7d). In particular, along PC2 we can clearly discriminate ammonia from all the other gases. Of note that the Gr_pristine sensor is the one showing the best response to ammonia, closely followed by the Gr_NiPc sample (see for instance Fig. 6-top panel). Regarding the discrimination between ethanol, acetone and 2-propanol, achieved only in the PC3–PC1 space, it is clear from the loadings on the component 3 that the central role is played by the Gr_NiPc, closely followed by Gr_CoPc and Gr_ZnPc (Fig. 7e). It is clear, as it is expected, that to obtain a good discrimination it is not mandatory to achieve high response from all the sensors to all gases, but response variability among sensing layers plays a crucial role.

PCA assesses the capability of the 5-sensors array to clearly discriminate all the tested gases in a 3D-space, making the array particularly promising for breathomics, environmental monitoring or food quality tracking application. All the sensors equally contribute to the discrimination capability, since PC3 is defined by Gr_NiPc, followed by Gr_CoPc contributions, PC2 is dominated by GR_pristine and, to less extent, to Gr_NiPc, while Gr_FePc and Gr_ZnPc mainly contribute to the PC1 discrimination.

Conclusion

The goal of the present study was to build the first e-nose based on a graphene chemiresistors array. Accordingly, we demonstrated that the device can be built and can operate as an e-nose with the required capability to selectively detect molecules in the gas phase. With the aim to create robust and chemically stable interfaces, we combined the sensing properties of M-Pc with the superior transport properties of Gr, by preparing four graphene layers functionalized with M-Pc. To create these interfaces, we chose drop-casting as a straightforward and low-cost method.

After AFM and Raman characterization, a sensor array was created with the four functionalized layers and a pristine Gr one in order to build the e-nose. The overall sensing behaviour of the prepared sensors has been investigated at first with exposures to ammonia. We drew the calibration curves and discussed the sensing mechanism in particular for the Gr_CoPc layer. Then, several exposures to ammonia, hydrogen sulfide, benzene, acetone, ethanol, 2-propanol, and water vapour have been carried out and the data have been used to feed the principal component analysis (PCA) and assess the discrimination capability of the device.

Of note, the tested concentrations of almost all gases are relevant for breathomics, where the biomarkers in the exhaled breath can be found in a concentration in a low-/sub-ppm range.[11,13,14,57,60,91,92]

All tested gases are clearly discriminated in a 3-dimensional PCA space. In particular, it is worth noting the capability of the array to detect VOCs that are usually poorly discriminated with chemiresistors, unless novel approaches for detection schemes and data handling are devised.[93]

Furthermore, we showed that an e-nose can be used for a parallel benchmarking of possible chemiresistors. Indeed, the possibility to test all the prepared samples on our e-nose simultaneously allowed us to point out the higher sensitivity of the Gr_ZnPC layer to benzene and hydrogen sulfide, and of Gr_FePC to 2-propanol and sodium hypochlorite with respect to the other chemiresistors equipping the e-nose.

So far, e-noses based on Gr chemiresitors have not yet been reported and therefore a benchmarking of our e-nose with similar devices is currently unfeasible. In this perspective, the present work represents a proof of concept, bridging the gap between graphene-based chemiresistors and e-noses. The low-cost and simple functionalization technique, as well as the easiness of use and simplicity of the electronic nose itself, make the presented array suitable and promising for environmental monitoring, food quality tracking and, especially, breathomics applications.

Author contributions

S. F.: investigation, methodology, formal analysis, visualization, validation, writing – original draft. C. M: investigation, formal analysis, writing – review and editing. S. P.: validation, writing – review and editing. G. D.: investigation, writing – review and editing. L. S.: conceptualization, methodology, funding, supervision, writing – review and editing.

Conflicts of interest

There are no conflicts to declare.

Acknowledgements

Authors acknowledge founding from the project "MADAM – Metal Activated 2D cArbon-based platforMs" funded by the MIUR Progetti di Ricerca di Rilevante Interesse Nazionale (PRIN) Bando 2017 – grant 2017NYPHN8. S. F. acknowledges Prof. Steven De Feyter for the fruitful discussions.

References

1 A. Staerz, F. Roeck, U. Weimar and N. Barsan, Electronic Nose: Current Status and Future Trends, in *Surface and Interface Science: Applications of Surface Science I*, ed. K. Wandelt, Wiley-VCH, 2020, pp. 335–379.

2 M. Khatib and H. Haick, Sensors for Volatile Organic Compounds, *ACS Nano*, 2022, **16**(5), 7080–7115.

3 L. Zhang, F. Tian and D. Zhang, *Electronic Nose: Algorithmic Challenges*, Springer, Singapore, 2018.

4 A. T. John, K. Murugappan, D. R. Nisbet and A. Tricoli, An outlook of recent advances in chemiresistive sensor-based electronic nose systems for food quality and environmental monitoring, *Sensors*, 2021, **21**(7), 2271.

5 W. Jia, G. Liang, Y. Wang and J. Wang, Electronic noses as a powerful tool for assessing meat quality: A mini review, *Food Anal. Methods*, 2018, **11**(10), 2916–2924.

6 M. Roy and B. K. Yadav, Electronic nose for detection of food adulteration: A review, *J. Food Sci. Technol.*, 2021, 1–13.

7 M. L. Rodríguez-Méndez, J. A. De Saja, R. González-Antón, C. García-Hernández, C. Medina-Plaza, C. García-Cabezón and F. Martín-Pedrosa, Electronic noses and tongues in wine industry, *Front. Bioeng. Biotechnol.*, 2016, **4**, 81.

8 M. Russo, D. Serra, F. Suraci, R. Di Sanzo, S. Fuda and S. Postorino, The potential of e-nose aroma profiling for identifying the geographical origin of licorice (Glycyrrhiza glabra L.) roots, *Food Chem.*, 2014, **165**, 467–474.

9 Y. Jian, W. Hu, Z. Zhao, P. Cheng, H. Haick, M. Yao and W. Wu, Gas sensors based on chemi-resistive hybrid functional nanomaterials, *Nano-Micro Lett.*, 2020, **12**(1), 1–43.

10 T. Saidi, O. Zaim, M. Moufid, N. El Bari, R. Ionescu and B. Bouchikhi, Exhaled breath analysis using electronic nose and gas chromatography–mass spectrometry for non-invasive diagnosis of chronic kidney disease, diabetes mellitus and healthy subjects, *Sens. Actuators, B*, 2018, **257**, 178–188.

11 S. Freddi, A. V. Emelianov, I. I. Bobrinetskiy, G. Drera, S. Pagliara, D. S. Kopylova, M. Chiesa, G. Santini, N. Mores, U. Moscato, A. G. Nasibulin, P. Montuschi and L. Sangaletti, Development of a Sensing Array for Human Breath Analysis Based on SWCNT Layers Functionalized with Semiconductor Organic Molecules, *Adv. Healthcare Mater.*, 2020, **9**, 200037.

12 C. Sánchez, J. P. Santos and J. Lozano, Use of electronic noses for diagnosis of digestive and respiratory diseases through the breath, *Biosensors*, 2019, **9**(1), 35.

13 R. Vishinkin and H. Haick, Nanoscale Sensor Technologies for Disease Detection via Volatolomics, *Small*, 2015, **11**, 6142.

14 C. Di Natale, R. Paolesse, E. Martinelli and R. Capuano, Solid-state gas sensors for breath analysis: A review, *Anal. Chim. Acta*, 2014, **824**, 1–17.

15 A. D. Wilson, M. Baietto Applications and Advances in Electronic-Nose Technologies, *Sensors*, 2009, **9**, 5099–5148.

16 G. Drera, S. Freddi, A. V. Emelianov, I. I. Bobrinetskiy, M. Chiesa, M. Zanotti, S. Pagliara, F. S. Fedorov, A. G. Nasibulin, P. Montuschi and L. Sangaletti, Exploring the performances of a functionalized CNT-based sensor array for breathomics through clustering and classification algorithms: from gas sensing of selective biomarkers to discrimination of chronic obstructive pulmonary disease, *RSC Adv.*, 2021, **11**, 30270–30282.

17 R. Ionescu, Y. Broza, H. Shaltieli, D. Sadeh, Y. Zilberman, X. Feng, L. Glass-Marmor, I. Lejbkowicz, K. Müllen, A. Miller and H. Haick, Detection of multiple sclerosis from exhaled breath using bilayers of polycyclic aromatic hydrocarbons and single-wall carbon nanotubes, *ACS Chem. Neurosci.*, 2011, **2**, 687.

18 I. Nardi-Agmon, M. Abud-Hawa, O. Liran, N. Gai-Mor, M. Ilouze, A. Onn, J. Bar, D. Shlomi, H. Haick and N. Peled, Exhaled breath analysis for monitoring response to treatment in advanced lung cancer, *J. Thorac. Oncol.*, 2016, **11**, 827.

19 H. Amal, M. Leja, K. Funka, R. Skapars, A. Sivins, G. Ancans, I. Liepniece-Karele, I. Kikuste, I. Lasina and H. Haick, Detection of precancerous gastric lesions and gastric cancer through exhaled breath, *Gut*, 2016, **65**, 400.

20 C. Wongchoosuk, A. Wisitsoraat, A. Tuantranont and T. Kerdcharoen, Portable electronic nose based on carbon nanotube-SnO2 gas sensors and its application for detection of methanol contamination in whiskeys, *Sens. Actuators, B*, 2010, **147**(2), 392–399.

21 V. Schroeder, E. D. Evans, Y. C. M. Wu, C. C. A. Voll, B. R. McDonald, S. Savagatrup and T. M. Swager, Chemiresistive sensor array and machine learning classification of food, *ACS Sens.*, 2019, **4**(8), 2101–2108.

22 F. Schedin, A. K. Geim, S. V. Morozov, E. W. Hill, P. Blake, M. I. Katsnelson and K. S. Novoselov, Detection of individual gas molecules adsorbed on graphene, *Nat. Mater.*, 2007, **6**(9), 652–655.

23 K. Toda, R. Furue and S. Hayami, Recent progress in applications of graphene oxide for gas sensing: A review, *Anal. Chim. Acta*, 2015, **878**, 43–53.

24 T. Wang, D. Huang, Z. Yang, S. Xu, G. He, X. Li, N. Hu, G. Yin, D. He and L. Zhang, A review on graphene-based gas/vapor sensors with unique properties and potential applications, *Nano-Micro Lett.*, 2016, **8**(2), 95–119.

25 F. Yin, W. Yue, Y. Li, S. Gao, C. Zhang, H. Kan, H. Niu, W. Wang and Y. Guo, Carbon-based nanomaterials for the detection of volatile organic compounds: A review, *Carbon*, 2021, **180**, 274–297.

26 G. Ambrosio, A. Brown, L. Daukiya, G. Drera, G. Di Santo, L. Petaccia, S. De Feyter, L. Sangaletti and S. Pagliara, Impact of covalent functionalization by diazonium chemistry on the electronic properties of graphene on SiC, *Nanoscale*, 2020, **12**(16), 9032–9037.

27 A. J. Marsden, P. Brommer, J. J. Mudd, M. A. Dyson, R. Cook, M. Asensio, J. Avila, A. Levy, J. Sloan, D. Quigley, G. R. Bell and N. R. Wilson, Effect of oxygen and nitrogen functionalization on the physical and electronic structure of graphene, *Nano Res.*, 2015, **8**(8), 2620–2635.

28 S. Freddi, M. C. Rodriguez Gonzalez, P. Carro, L. Sangaletti and S. De Feyter, Chemical defect-driven response on graphene-based chemiresistors for sub-ppm ammonia detection, *Angew. Chem., Int. Ed.*, 2022, **61**(16), e202200115.

29 S. Freddi, D. Perilli, L. Vaghi, M. Monti, A. Papagni, C. Di Valentin and L. Sangaletti, Pushing down the limit of NH_3 detection of graphene-based chemiresistive sensors through functionalization by thermally activated tetrazoles dimerization, *ACS Nano*, 2022, **16**(7), 10456–10469.

30 N. Alzate-Carvajal and A. Luican-Mayer, Functionalized Graphene Surfaces for Selective Gas Sensing, *ACS Omega*, 2020, **5**, 21320–21329.

31 K. Sawada, T. Tanaka, T. Yokoyama, R. Yamachi, Y. Oka, Y. Chiba, *et al.*, Co-porphyrin functionalized CVD graphene ammonia sensor with high selectivity to disturbing gases: hydrogen and humidity, *Jpn. J. Appl. Phys.*, 2020, **59**, SGGG09.

32 C. Mackin, V. Schroeder, A. Zurutuza, C. Su, J. Kong, T. M. Swager and T. Palacios, Chemiresistive graphene sensors for ammonia detection, *ACS Appl. Mater. Interfaces*, 2018, **10**, 16169–16176.

33 T. Hayasaka, A. Lin, V. C. Copa, L. P. Lopez, R. A. Loberternos, L. I. M. Ballesteros, *et al.*, An electronic nose using a single graphene FET and machine learning for water, methanol, and ethanol, *Microsyst. Nanoeng.*, 2020, **6**(1), 1–13.

34 H. Liu, Y. Chu, Y. Liu, T. Hayasaka, N. Joshi, Y. Cui, *et al.*, Selective sensing of chemical vapors using phase spectra detection on CVD graphene fet, in *IEEE Micro Electro Mechanical Systems (MEMS)*, 2018, pp. 210–213.

35 A. Inaba, Y. Takei, K. Matsumoto and I. Shimoyama, Ionic liquid-gated graphene FET array with enhanced selectivity for electronic nose, in *IEEE 27th International Conference on Micro Electro Mechanical Systems (MEMS)*, 2014, pp. 326–329.

36 N. S. Capman, X. V. Zhen, J. T. Nelson, V. S. K. Chaganti, R. C. Finc, M. J. Lyden, *et al.*, Machine Learning-Based Rapid Detection of Volatile Organic Compounds in a Graphene Electronic Nose, *ACS Nano*, 2022, **16**(11), 19567–19583.

37 F. I. Bohrer, C. N. Colesniuc, J. Park, M. E. Ruidiaz, I. K. Schuller, A. C. Kummel and W. C. Trogler, Comparative Gas Sensing in Cobalt, Nickel, Copper, Zinc, and Metal-Free Phthalocyanine Chemiresistors, *J. Am. Chem. Soc.*, 2009, **131**, 478–485.

38 F. I. Bohrer, A. Sharoni, C. Colesniuc, J. Park, I. K. Schuller, A. C. Kummel and W. C. Trogler, Gas Sensing Mechanism in Chemiresistive Cobalt and Metal-Free Phthalocyanine Thin Films, *J. Am. Chem. Soc.*, 2007, **129**, 5640–5646.

39 K.-C. Ho and Y.-H. Tsou, Chemiresistor-type NO gas sensor based on nickel phthalocyanine thin films, *Sens. Actuators, B*, 2010, **77**, 253–259.

40 A. M. Datir, V. S. Ghole, P. Koinkar and S. D. Chakane, Nitrogen dioxide gas sensor based on cobalt and nickel phthalocyanine working at room temperature, *Int. J. Mod. Phys. B*, 2011, **25**, 4190–4193.

41 T. Sizun, M. Bouvet, Y. Che, J.-M. Suisse, G. Barochi and J. Rossignol, Differential study of substituted and unsubstituted cobalt phthalocyanines for gas sensor applications, *Sens. Actuators, B*, 2011, **159**, 163–170.

42 X. Li, Y. Jiang, G. Xie, H. Tai, P. Sun and B. Zhang, Copper phthalocyanine thin film transistors for hydrogen sulfide detection, *Sens. Actuators, B*, 2013, **176**, 1191–1196.

43 X. Wan, X. Wang, J. Gao and B. Xu, Iron phthalocyanine nanorods for ethanol sensoring, *Micro Nano Lett.*, 2016, **11**(7), 348–350.

44 D. D. Klyamer, A. S. Sukhikh, P. O. Krasnov, S. A. Gromilov, N. B. Morozova and T. V. Basova, Thin films of tetrafluoro substituted cobalt phthalocyanine: Structure and sensor properties, *Appl. Surf. Sci.*, 2016, **372**, 79–86.

45 M. Kaur, R. Kumar, R. Dogra, N. Arora and N. Sharma, Characterization of drop-cast copper phthalocyanine thin films for ammonia sensing, *Surf. Innovations*, 2018, **6**(4–5), 295–300.

46 R. Rella, A. Serra, P. Siciliano, A. Tepore, L. Valli and A. Zocco, Effects of NO2 oxidizing gas on a novel phthalocyanine Langmuir-Blodgett thin film, *Thin Solid Films*, 1996, **286**, 256–258.

47 P. B. M. Archer, A. V. Chadwick, J. J. Miasik, M. Tamizi and J. D. Wright, Kinetic factors in the response of organometallic semiconductor gas sensors, *Sens. Actuators*, 1989, **16**, 379–392.

48 M. K. Rana, M. Sinha and S. Panda, Gas sensing behavior of metal-phthalocyanines: Effects of electronic structure on sensitivity, *Chem. Phys.*, 2018, **513**, 23–34.

49 L. S. Chia, Y. H. Du, S. Palale and P. S. Lee, Interaction of Copper Phthalocyanine with Nitrogen Dioxide and Ammonia Investigation Using X-ray Absorption Spectroscopy and Chemiresistive Gas Measurements, *ACS Omega*, 2019, **4**, 10388–10395.

50 S. Kumar, N. Kaur, A. K. Sharma, A. Mahajan and R. K. Bedi, Improved Cl2 sensing characteristics of reduced graphene oxide when decorated with copper phthalocyanine nanoflowers, *RSC Adv.*, 2017, **7**, 25229.

51 X. Zhou, X. Wang, B. Wang, Z. Chen, C. He and Y. Wu, Preparation, characterization and NH3-sensing properties of reducedgraphene oxide/copper phthalocyanine hybrid material, *Sens. Actuators, B*, 2014, **193**, 340–348.

52 X. Zhang, Y. Feng, S. Tang and W. Feng, Preparation of a graphene oxide–phthalocyanine hybrid through strong π-π interactions, *Carbon*, 2010, **48**, 211–216.

53 D. Klyamer, R. Shutilov and T. Basova, Recent Advances in Phthalocyanine and Porphyrin-Based Materials as Active Layers for Nitric Oxide Chemical Sensors, *Sensors*, 2022, **22**(3), 895.

54 E. N. Kaya, A. Şenocak, D. D. Klyamer, E. Demirbaş, T. V. Basova and M. Durmuş, Ammonia sensing performance of thin films of cobalt (II) phthalocyanine bearing fluorinated substituents, *J. Mater. Sci.: Mater. Electron.*, 2019, **30**(8), 7543–7551.

55 M. Bouvet, Phthalocyanine-based field-effect transistors as gas sensors, *Anal. Bioanal. Chem.*, 2006, **384**(2), 366–373.

56 K.-C. Ho and Y.-H. Tsou, Chemiresistor-type NO gas sensor based on nickel phthalocyanine thin films, *Sens. Actuators, B*, 2001, **77**(1), 253–259.

57 L. R. Narasimhan, W. Goodman, C. Kumar and N. Patel, Correlation of breath ammonia with blood urea nitrogen and creatinine during hemodialysis, *Proc. Natl. Acad. Sci. U. S. A.*, 2001, **98**, 4617.

58 M.-Y. Chuang, C. C. Chen, H.-W. Zan, H.-F. Meng and C.-J. Lu, Organic gas sensor with an improved lifetime for detecting breath ammonia in hemodialysis patients, *ACS Sens.*, 2017, **2**, 1788.

59 J. Kong, N. R. Franklin, C. Zhou, M. G. Chapline, S. Peng, k. Cho and H. Dai, Nanotube molecular wires as chemical sensors, *Science*, 2000, **287**, 622.

60 G.-T. Fan, C.-L. Yang, C.-H. Lin, C.-C. Chen and C.-H. Shih, Applications of Hadamard transform-gas chromatography/mass spectrometry to the detection of acetone in healthy human and diabetes mellitus patient breath, *Talanta*, 2014, **120**, 386.

61 C. Turner, C. Walton, S. Hoashi and M. Evans, Breath acetone concentration decreases with blood glucose concentration in type I diabetes mellitus patients during hypoglycaemic clamps, *J. Breath Res.*, 2009, **3**, 046004.

62 S. Nag, A. Sachan, M. Castro, V. Choudhary and J. F. Feller, Sulfonated poly (ether-ether-ketone)[SPEEK] nanocomposites based on hybrid nanocarbons for the detection and discrimination of some lung cancer VOC biomarkers, *J. Mater. Chem. B*, 2017, **5**, 348.

63 P. Wang, G. Zhang, T. Wondimu, B. Ross and R. Wang, Hydrogen sulfide and asthma, *Exp. Physiol.*, 2011, **96**, 847.

64 Y. Suzuki, J. Saito, M. Uematsu, A. Fukuhara, S. Sato, R. Togawa, Y. Sato, K. Misa, T. Nikaido, N. Fukuhara, X. Wang, Y. Tanino and M. Munakata, Clinical application of hydrogen sulfide (H2S) as a marker of asthma management, *Eur. Respir. J.*, 2016, **48**, PA3379.

65 A. Zacharasiewicz, N. Wilson, C. Lex, A. Li, M. Kemp, J. Donovan, J. Hooper, S. A. Kharitonov and A. Bush, Repeatability of sodium and chloride in exhaled breath condensates, *Pediatr. Pulmonol.*, 2004, **37**, 273.

66 F. Ghani, J. Kristen and H. Riegler, Solubility Properties of Unsubstituted Metal Phthalocyanines in Different Types of Solvents, *J. Chem. Eng. Data*, 2012, **57**, 439–449.

67 Gwyddion, accessed: February, 2022, **https://gwyddion.net/**.

68 A. C. Ferrari and D. M. Basko, Raman spectroscopy as a versatile tool for studying the properties of graphene, *Nat. Nanotechnol.*, 2013, **8**, 235–246.

69 J. Z. Jiang, K. Stahl, R. W. Berg, D. J. Frost, T. J. Zhou and P. X. Shi, Structural characterization of cubic silicon nitride, *Europhys. Lett.*, 2000, **51**, 62.

70 C. Murray, N. Dozova, J. G. McCaffrey, S. FitzGerald, N. Shafizadeh and C. Crepin, Infra-red and Raman spectroscopy of free-base and zinc phthalocyanines isolated in matrices, *Phys. Chem. Chem. Phys.*, 2010, **12**, 10406–10422.

71 D. Kumar, P. Chaturvedi, P. Saho, P. Jha, A. Chouksey, M. Lal, J. S. B. S. Rawat, R. P. Tandon and P. K. Chaudhury, Effect of single wall carbon nanotube networks on gas sensor response and detection limit, *Sens. Actuators, B*, 2017, **240**, 1134–1140.

72 F. Rigoni, S. Freddi, S. Pagliara, G. Drera, L. Sangaletti, J.-M. Suisse, M. Bouvet, A. M. Malovichko, A. V. Emelianov and I. Bobrinetskiy, Humidity-enhanced sub-ppm sensitivity to ammonia of covalently functionalized singlewall carbon nanotube bundle layers, *Nanotechnology*, 2017, **28**, 255502.

73 M. Gautam and A. H. Jayatissa, Ammonia gas sensing behavior of graphene surface decorated with gold nanoparticles, *Solid-State Electron.*, 2012, **78**, 159–165.

74 F. Javari, E. Castillo, H. Gullapalli, P. M. Ajayan and N. Koratkar, High sensitivity detection of NO_2 and NH_3 in air using chemical vapor deposition grown graphene, *Appl. Phys. Lett.*, 2012, **100**, 203120.

75 Z. Wu, X. Chen, S. Zhu, Z. Zhou, Y. Yao, W. Quan and B. Liu, Enhanced sensitivity of ammonia sensor using graphene/polyaniline nanocomposite, *Sens. Actuators, B*, 2013, **178**, 485–493.

76 C. Xiang, D. Jiang, Y. Zou, H. Chu, S. Qiu, H. Zhang, F. Xu, L. Sun and L. Zheng, Ammonia sensor based on polypyrrole–graphene nanocomposite decorated with titania nanoparticles, *Ceram. Int.*, 2015, **41**, 6432–6438.

77 R. Lv, G. Chend, Q. Lie, A. McCreary, A. Botello-Méndez, S. V. Morozov, L. Liang, X. Declerck, N. Perea-López, D. A. Cullen, S. Feng, A. L. Elías, R. Cruz-Silva, K. Fujisawa, M. Endo, F. Kang, J.-C. Charlier, V. Meunier, M. Pan, A. R. Harutyunyan, K. S. Novoselov and M. Terrones, Ultrasensitive gas detection of large-area boron-doped graphene, *Proc. Natl. Acad. Sci. U. S. A.*, 2015, **112**, 14527–14532.

78 D. Wu, Q. Peng, S. Wu, G. Wang, L. Deng, H. Tai, L. Wang, Y. Yang, L. Dong, Y. Zhao, J. Zhao, D. Sun and L. Lin, A Simple Graphene NH_3 Gas Sensor via Laser Direct Writing, *Sensors*, 2018, **18**, 4405.

79 T. Liang, R. Liu, C. Lei, K. Wang, Z. Li and Y. Li, Preparation and Test of NH3 Gas Sensor Based on Single-Layer Graphene Film, *Micromachines*, 2020, **11**, 965.

80 S. Srivastava, S. K. Jain, G. Gupta, T. D. Senguttuvan and B. K. Gupta, Boron-doped few-layer graphene nanosheet gas sensor for enhanced ammonia sensing at room temperature, *RSC Adv.*, 2020, **10**, 1007.

81 X. Zhou, X. Wang, B. Wang, Z. Chen, C. He and Y. Wu, Preparation, characterization and NH_3-sensing properties of reduced graphene oxide/copper phthalocyanine hybrid material, *Sens. Actuators, B*, 2014, **193**, 340–348.

82 X. Li, B. Wang, X. Wang, X. Zhou, Z. Chen, C. He, Z. Yu and Y. Wu, Enhanced NH3-Sensitivity of Reduced Graphene Oxide Modified by Tetra-α-Iso-Pentyloxymetallophthalocyanine Derivatives, *Nanoscale Res. Lett.*, 2015, **10**, 373.

83 M. S. Polyakov, T. V. Basova, M. Göksel, A. Şenocak, E. Demirbaş, M. Durmuş, B. Kadem and A. Hassan, Effect of covalent and non-covalent linking of zinc(II) phthalocyanine functionalised carbon nanomaterials on the sensor response to ammonia, *Synth. Met.*, 2017, **227**, 78–86.

84 Z. Guo, B. Wang, X. Wang, Y. Li, S. Gai, Y. Wu and X. Cheng, A high-sensitive room temperature gas sensor based on

cobalt phthalocyanines and reduced graphene oxide nanohybrids for the ppb-levels of ammonia detection, *RSC Adv.*, 2019, **9**, 37518.

85 J. Ren, S. Meng, Y. L. Wang, X. C. Ma, Q. K. Xue and E. Kaxiras, Properties of copper (fluoro-) phthalocyanine layers deposited on epitaxial graphene, *J. Chem. Phys.*, 2011, **134**(19), 194706.

86 A. Casotto, G. Drera, D. Perilli, S. Freddi, S. Pagliara, M. Zanotti, L. Schio, A. Verdini, L. Floreano, C. Di Valentin and L. Sangaletti, π-Orbital Mediated Charge Transfer Channels in a Monolayer Gr-NiPc Heterointerface Unveiled by Soft X-Ray Electron Spectroscopies and DFT Calculations, *Nanoscale*, 2022, **14**, 13166–13177.

87 H. S. Soliman, M. M. El Nahass, A. M. Farid, A. A. M. Farag and A. A. El Shazly, Structural and transport properties of evaporated iron phthalocyanine (FePc) thin films, *Eur. Phys. J.: Appl. Phys.*, 2003, **21**(3), 187–193.

88 E. Aktas, J. Jiménez-López, K. Azizi, T. Torres and E. Palomares, Self-assembled Zn phthalocyanine as a robust p-type selective contact in perovskite solar cells, *Nanoscale Horiz.*, 2020, **5**(10), 1415–1419.

89 S. Freddi, G. Drera, S. Pagliara, A. Goldoni and L. Sangaletti, Enhanced selectivity of target gas molecules through a minimal array of gas sensors based on nanoparticle-decorated SWCNTs, *Analyst*, 2019, **144**(13), 4100–4110.

90 S. F. Liu, L. C. H. Moh and T. M. Swager, Single-walled carbon nanotube–metalloporphyrin chemiresistive gas sensor arrays for volatile organic compounds, *Chem. Mater.*, 2015, **27**, 3560.

91 S. Freddi and L. Sangaletti, Trends in the Development of Electronic Noses Based on Carbon Nanotubes Chemiresistors for Breathomics, *Nanomaterials*, 2022, **12**(7), 2992.

92 S. Abdulla, J. Dhakshinamoorthy, V. Mohan, D. V. Ponnuvelu, V. K. Kallidaikuruchi, L. M. Thalakkotil and B. Pullithadathil, Development of low-cost hybrid multi-walled carbon nanotube-based ammonia gas-sensing strips with an integrated sensor read-out system for clinical breath analyzer applications, *J. Breath Res.*, 2019, **13**(4), 046005.

93 S. Acharyya, S. Nag, S. Kimbahune, A. Ghose, A. Pal and P. K. Guha, Selective Discrimination of VOCs Applying Gas Sensing Kinetic Analysis over a Metal Oxide-Based Chemiresistive Gas Sensor, *ACS Sens.*, 2021, **6**(6), 2218–2224.